ACS APPLIED MATERIALS & INTERFACES

Applications of Polymer, Composite, and Coating Materials

Highly Efficient and Reliable Transparent Electromagnetic Interference Shielding Film

Li-Chuan Jia, Ding-Xiang Yan, Xiaofeng Liu, Rujun Ma, Hong-Yuan Wu, and Zhongming Li

ACS Appl. Mater. Interfaces, **Just Accepted Manuscript** • DOI: 10.1021/acsami.8b00492 • Publication Date (Web): 20 Mar 2018

Just Accepted

ACS Publications

is published by the American Chemical Society. 1155 Sixteenth Street N.W., Washington, DC 20036

Highly Efficient and Reliable Transparent Electromagnetic Interference Shielding Film

Li-Chuan Jia,[†] Ding-Xiang Yan,*[,‡] Xiaofeng Liu,[§] Rujun Ma,[§] Hong-Yuan Wu[†] and Zhong-Ming Li*[,†]

[†]College of Polymer Science and Engineering, State Key Laboratory of Polymer Materials Engineering, Sichuan University, Chengdu 610065, China

[‡]School of Aeronautics and Astronautics, Sichuan University, Chengdu 610065, China

[§]Department of Materials Science and Engineering, Henry Samueli School of Engineering and Applied Science, University of California, Los Angeles, CA 90095, USA

ABSTRACT: Electromagnetic protection in optoelectronic instruments such as optical windows and electronic displays is challenging because of the essential requirements of a high optical transmittance and an electromagnetic interference (EMI) shielding effectiveness (SE). Herein, we demonstrate the creation of an efficient transparent EMI shielding film that is composed of calcium alginate (CA), silver nanowires (AgNWs), and polyurethane (PU), *via* a facile and low-cost Meyer-rod coating method. The CA/AgNWs/PU film with a high optical transmittance of 92% achieves an EMI SE of 20.7 dB, which meets the requirements for commercial shielding applications. A superior EMI SE of 31.3 dB could be achieved, whereas the transparent film still maintains a transmittance of 81%. The integrated efficient EMI SE and high transmittance is superior to most previously reported transparent EMI shielding materials. Moreover, our transparent films exhibit a highly reliable shielding ability in a complex service environment, with 98% and 96% EMI SE retentions even after 30 min of ultrasound treatment and 5000 bending cycles (1.5-mm radius), respectively. The comprehensive performance that is associated with the facile fabrication strategy imparts the CA/AgNW/PU film with great potential as an optimized EMI shielding material in emerging optoelectronic devices, such as flexible solar cells, displays, and touch panels.

KEYWORDS: AgNW networks, EMI shielding, optical transmittance, flexible, reliable

1. INTRODUCTION

The flourishing development of electronic instruments and telecommunication devices generates severe electromagnetic radiation, which deteriorates nearby device performance, and threatens human health.[1–5] To reduce such an undesirable impact, electromagnetic interference (EMI) shielding materials, such as metal films, carbon-based papers, and conductive polymer composites, have been investigated extensively.[6–15] To satisfy the shielding requirement in visual windows and electronic displays for aeronautic, medical, civilian, and research facilities, the development of an EMI shielding material with a high optical transmittance, a superior EMI shielding effectiveness (EMI SE), and sufficient shielding reliability is imperative.[16-19] Indium-tin-oxide (ITO) films have served as transparent EMI shielding materials for a long time. Despite a favorable EMI SE and transmittance (30 dB @ 80%),[20] ITO films are brittle and indium sources are scarce and expensive. Other transparent EMI shielding materials have also been investigated, such as monolayer graphene film (2.3 dB @ 97%),[21] aluminum-doped ZnO film (6.5 dB @ 83.2%),[22] and polyaniline film (5.8 dB @ 58%).[23] Apparently, a limited EMI SE was reported, despite adequate transmittance. Graphene/polymer films with interleaved and multi-layer structures were developed for an improved EMI SE compared with monolayer graphene film, but these had a reduced transmittance.[24,25] Recently, favorable outcomes were obtained in a crackle-template-based metallic mesh (26.0 dB @ 91%) and a graphene/metallic mesh/transparent dielectric hybrid shielding material (35.2 dB @ 91%), with the assistance of chemical vapor deposition and ultraviolet

photolithography methods.[16,26] However, the shielding reliability of these previously reported EMI shielding materials has rarely been reported, which is extremely important for their practical applications in curved screens and roll-up displays where mechanical deformations are necessary.

Silver nanowires (AgNWs) have been demonstrated as promising materials to prepare transparent and reliable conductors because of their intrinsically high conductivity, large aspect ratio, and good mechanical flexibility.[27–30] Recently, AgNW-based conductors have been applied in transparent electrodes, flexible energy devices, stretchable sensors, environmental science, touch screens, organic light-emitting diodes, and transparent heaters.[31-49] Hu *et al*. reported transparent EMI shielding in a poly(ethersulfone)/AgNWs/polyethylene terephthalate film, which exhibited an EMI SE of 23 dB and a transmittance of 81%.[50] Polyethylene oxide (PEO) was used primarily to assist in the formation of a AgNW film and a high-heat-treatment process was required to remove the PEO thereafter. Very recently, a highly stretchable and transparent AgNWs/poly(dimethylsiloxane) shielding film was developed by vacuum filtration and transfer method, showing an EMI SE of 20 dB and a transmittance of 93.8%. Whereas, the fabricated method endure the shortcomings in inefficiency and sophistication, which made their large-scale production difficult.[51]

Herein, we demonstrate the facile fabrication of a highly efficient and reliable transparent EMI shielding film with AgNW percolation networks that are embedded between calcium alginate (CA) and polyurethane (PU), *via* a Meyer-rod coating

method. The CA/AgNWs/PU film achieves a satisfactory EMI SE of 20.7 dB with a high optical transmittance of 92% at an AgNW area density of 58 mg/m^2. A higher EMI SE of 31.3 dB is achieved at an increased AgNW area density, with a transmittance of 81%. The encapsulation structure of the AgNW networks and its mechanical flexibility allow such a film to maintain a superior EMI shielding ability even after 30 min of ultrasound treatment and 5000 bending cycles. These results demonstrate that CA/AgNWs/PU films can serve as promising transparent EMI shielding materials for emerging optoelectronic devices, such as flexible solar cells, displays, and touch panels.

2. EXPERIMENTAL SECTION

2.1. Materials

The AgNW dispersion was purchased from Zhejiang Kechuang Advanced Materials Co., Ltd, with an average diameter of 30 nm and an average length of 15 μm (Zhejiang, China). PU was prepared from a urethane liquid rubber compound with part A component (4,4′ methylenedicyclohexyl diisocyanate) and part B component (phenylmercury neodecanoate) (Clear Flex® 95, Smooth-On, Inc., Pennsylvania, USA). Sodium alginate (SA), calcium chloride ($CaCl_2$), isopropyl alcohol (IPA), and deionized water were purchased from Chengdu Kelong Chemical Reagent Factory (Chengdu, China). Polyethylene terephthalate (PET) film was supplied by Chengdu Junkai Packaging Co. LTD (Chengdu, China).

2.2. CA/AgNWs/PU film fabrication

The CA/AgNWs/PU film fabrication included four main steps. First, SA was

dissolved in deionized water and the SA solution (2.0 wt%) was blade-coated onto a glass substrate. SA film was obtained after drying at 60 °C for 10 min. Then AgNW dispersion (5 mg/mL) was dropped on the edge of a SA film, and a Mayer rod #6 (R.D. Specialties, Inc., USA) was rolled immediately over the drops to spread the AgNW dispersion over the film surface, followed by air-drying. The compounded liquid PU was blade-coated onto the AgNW surface and cured at 25 °C for 24 h. The SA/AgNWs/PU film was peeled from the glass substrate and immersed into $CaCl_2$/deionized water solution (10 wt%) to prepare the CA/AgNWs/PU film. The CA/AgNWs/PU film was rinsed with excess deionized water and dried at 60 °C for 10 h. An AgNW area density (namely the AgNW weight per unit area of the circuit) was introduced to evaluate the distribution density of AgNW networks in the CA/AgNWs/PU film, which was calculated based on the AgNW wet-film thickness and the AgNW dispersion concentration. The AgNW area density was 58 mg/m^2 for one deposition of AgNW dispersion by the Mayer-rod technique and can be adjusted by increasing the deposition times. For comparison, a transparent EMI shielding AgNWs/PET film was fabricated by a spray-coating technique. An air brush (HP-CP Iwata, Japan) with a 0.2-mm nozzle was used to deposit the AgNW dispersion onto a PET substrate, which was resting on a hotplate (80 °C). The spraying distance, moving speed, and spraying pressure of the nozzle were 15 cm, 2 cm/s, and 0.2 MPa, respectively.

2.3. Characterization

The surface morphologies of the AgNW percolated networks were observed by using

a field emission scanning electron microscopy (FE-SEM, Inspect-F, FEI, USA), at an accelerating voltage of 5.0 kV. Cross-sections for the SEM observations were obtained by cryo-fracturing the specimens after rapid immersion in liquid nitrogen for 30 min beforehand. The cross-sections were coated with a thin layer of gold. The sheet resistance (Rs) was measured by using a four-point probe (RTS-8, Guangzhou Four-Point Probe Technology Co., Ltd., China). Since the CA is non-conducting and thus we measured the Rs of AgNW networks on the SA film surface to characterize the electrical performance of the CA/AgNWs/PU films. The transmittance spectra of the CA/AgNWs/PU films were recorded on a UV–visible spectrophotometer (UV-3600, Shimadzu, Japan). EMI shielding measurements were performed with a coaxial test cell (APC-7 connector) in conjunction with an Agilent N5247A vector network analyzer, according to ASTM ES7-83 and ASTM D4935-99 (Schematic of measurement setup was shown in our previous work).[52] Samples with a 10-mm diameter were placed in the specimen holder, which is connected to separate the VNA ports through an Agilent 85132F coaxial line. The APC-7 connector is a precision coaxial connector that can be used on laboratory microwave test equipment for frequencies up to 18 GHz. Scattering parameters (S_{11} and S_{21}) of the PU-AgNWs/Textile in C-band (4-8 GHz), X-band (8.2-12.4 GHz) and Ku-band (12.4-18 GHz) were obtained to calculate the EMI SE. A detailed calculation of the SE_R, SE_A, and SE_M is provided in the Supporting Information. To evaluate the EMI shielding reliability of the CA/AgNWs/PU film and the comparative AgNWs/PET film, the EMI SE of these two films was measured after 30 min of ultrasonic

treatment and repeated bending deformation. The bending processes were performed manually for 2 s for each cycle at a 1.5-mm radius, and required ~3 h for the 5000 cycles.

3. RESULTS AND DISCUSSION

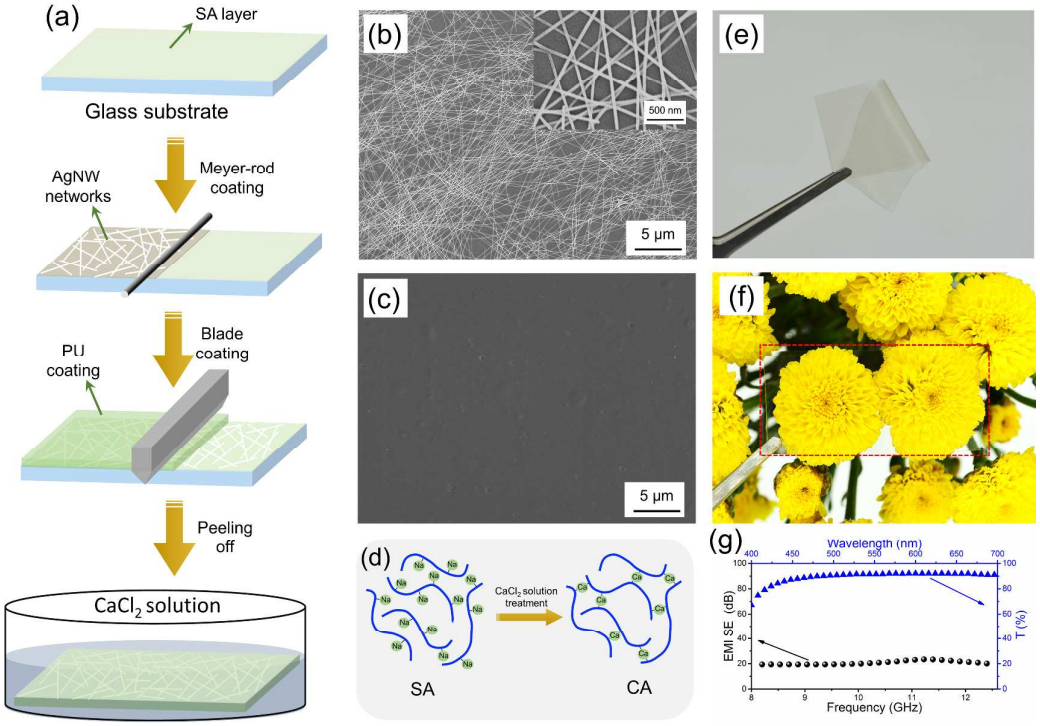

Figure 1 (a) Schematic procedure to fabricate the CA/AgNWs/PU film. (b) SEM image of AgNWs on SA film surface after Meyer-rod coating with one AgNW dispersion deposition. The inset shows the corresponding magnified image. (c) SEM image of the SA layer surface for the SA/AgNWs/PU film. (d) Schematic diagram for the transformation of SA to CA. (e, f) Digital photographs of CA/AgNWs/PU film. The sample lies in the red dotted frame. (g) The optical transmittance and EMI SE of the CA/AgNWs/PU film at an AgNW area density of 58 mg/m^2.

The fabrication of the CA/AgNWs/PU film is shown in Figure 1a. First, a 3 μm-thick

SA film was formed on the clean glass substrate *via* blade coating. SA was chosen as the overcoating layer due to its good film formability. The AgNW dispersion was deposited and spread over the SA film using the Mayer-rod coating technique. The AgNW area density is 58 mg/m^2 for one deposition of AgNW dispersion and can be adjusted easily by increasing the deposition times, as detailed in the Experimental Section. Figure 1b shows typical SEM images of AgNW networks on the SA film surface. AgNWs are distributed randomly without obvious aggregation and the junctions between the AgNWs are well established (inset of Figure 1b), which indicates the formation of high-quality AgNW networks. The compounded liquid PU was blade-coated and penetrated the interconnected pores of the AgNW networks. After being cured at 25 °C for 24 h, the formed SA/AgNWs/PU film can be peeled easily from the glass substrate without any damage to the SA layer surface (Figure 1c). Considering the fact that the inherent aqueous solubility of SA would make the SA layer in the SA/AgNWs/PU film easily scraped off by something containing water and thus affect the comprehensive film performance, the water-soluble SA was transformed into a water-insoluble CA by immersing the SA/AgNWs/PU film into a $CaCl_2$ solution, as shown schematically in Figure 1d. The resultant film was marked as a CA/AgNWs/PU film. The digital photographs in Figure 1e and f show the excellent mechanical flexibility and optical transmittance of the CA/AgNWs/PU film. Figure 1g shows the optical transparency *vs* wavelength-dependent and EMI SE *vs* frequency behaviors of the CA/AgNWs/PU film at an AgNW area density of 58 mg/m^2. The optical transmittance at 550 nm and the average EMI SE are 92% and

20.7 dB, which is sufficient for the practical application of such films in optoelectronic systems, such as smart windows and flexible displays. More details on the transparent and EMI shielding performance will be discussed later.

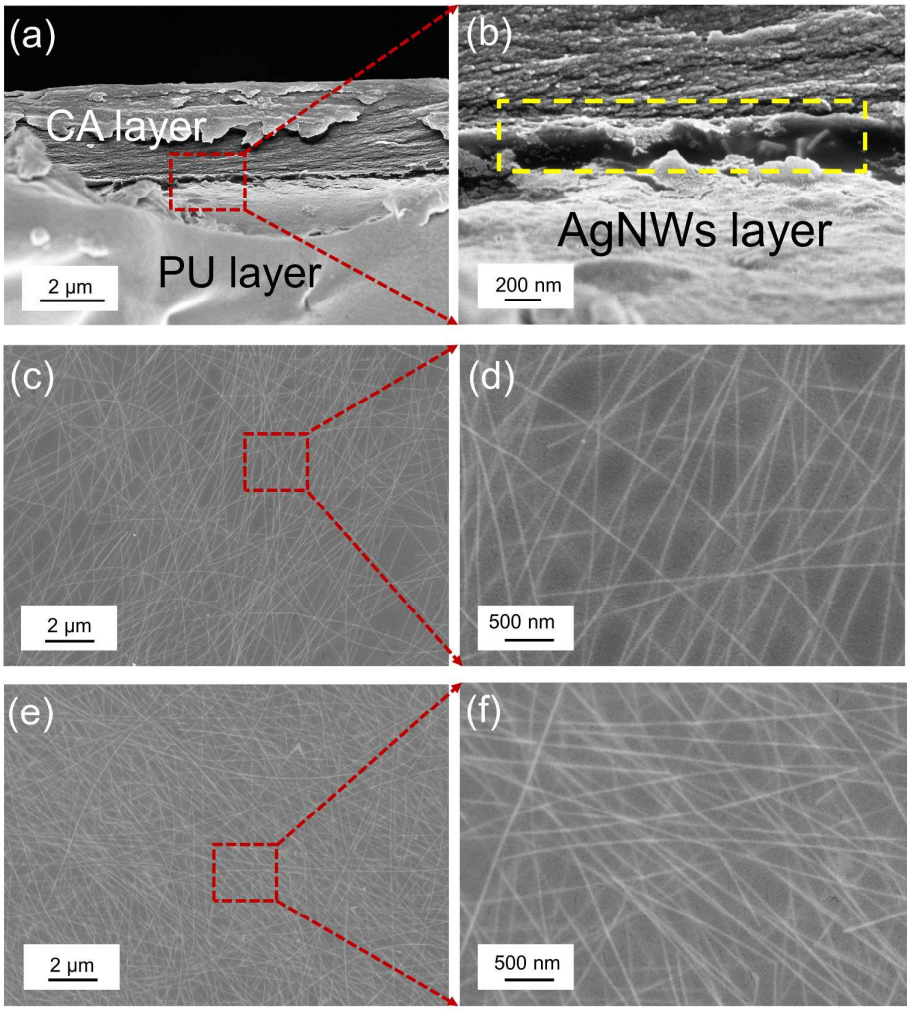

Figure 2 (a, b) Cross-sectional SEM images of the CA/AgNWs/PU film, at an AgNW area density of 174 mg/m^2. (c, d) SEM images of SA/AgNWs/PU film surface after etching a SA layer. The AgNW area density is 58 mg/m^2. (e, f) SEM images of SA/AgNWs/PU film surface after etching a SA layer. The AgNW area density is 174 mg/m^2.

AgNW networks are extremely important for the transparent and electrical

performance of the final CA/AgNWs/PU film. Cross-sectional SEM images (Figure 2a and b) reveal the formation of a sandwich-like structure with the encapsulation of AgNW networks between the CA and PU layers. The typical sandwich-like structure would impart the CA/AgNWs/PU film with unique characteristics, such as strong resistance to exfoliation and anti-oxidation because of a firm anchoring effect of the polymer layers to the AgNW networks.[53] To study the in-plane distribution state of the AgNW networks in the CA/AgNWs/PU film, one should etch the CA or PU layer to make the AgNW surface visual. Because of the good solvent resistance of the CA and the cross-linked structure of the PU, the CA or PU layer is difficult to etch. Thus, we chose a precursor of the CA/AgNWs/PU film, *i.e.*, the SA/AgNWs/PU film as the target. The SA layer in the SA/AgNWs/PU film was etched by using deionized water and the corresponding SEM images of the AgNW surface are shown in Figure 2c–f. Individual AgNW with a high aspect ratio is visible, which constructs connected conductive paths throughout the surface. For the film with a 58 mg/m^2 AgNW area density, the AgNW networks on the PU layer (Figure 2c and d) are similar to the deposited AgNW networks on the SA surface (Figure 1b), which indicates that the introduction of a PU layer does not damage the well-established conductive AgNW networks. As the AgNW area density increases to 174 mg/m^2 (Figure 2e), more AgNW junctions are formed, which would provide more electron transfer paths. The higher-magnification SEM images (Figure 2d and f) show that AgNWs are embedded in the PU layer. This phenomenon is attributed to the permeation of liquid PU into the pores of the AgNW networks when it coated the AgNW surface.

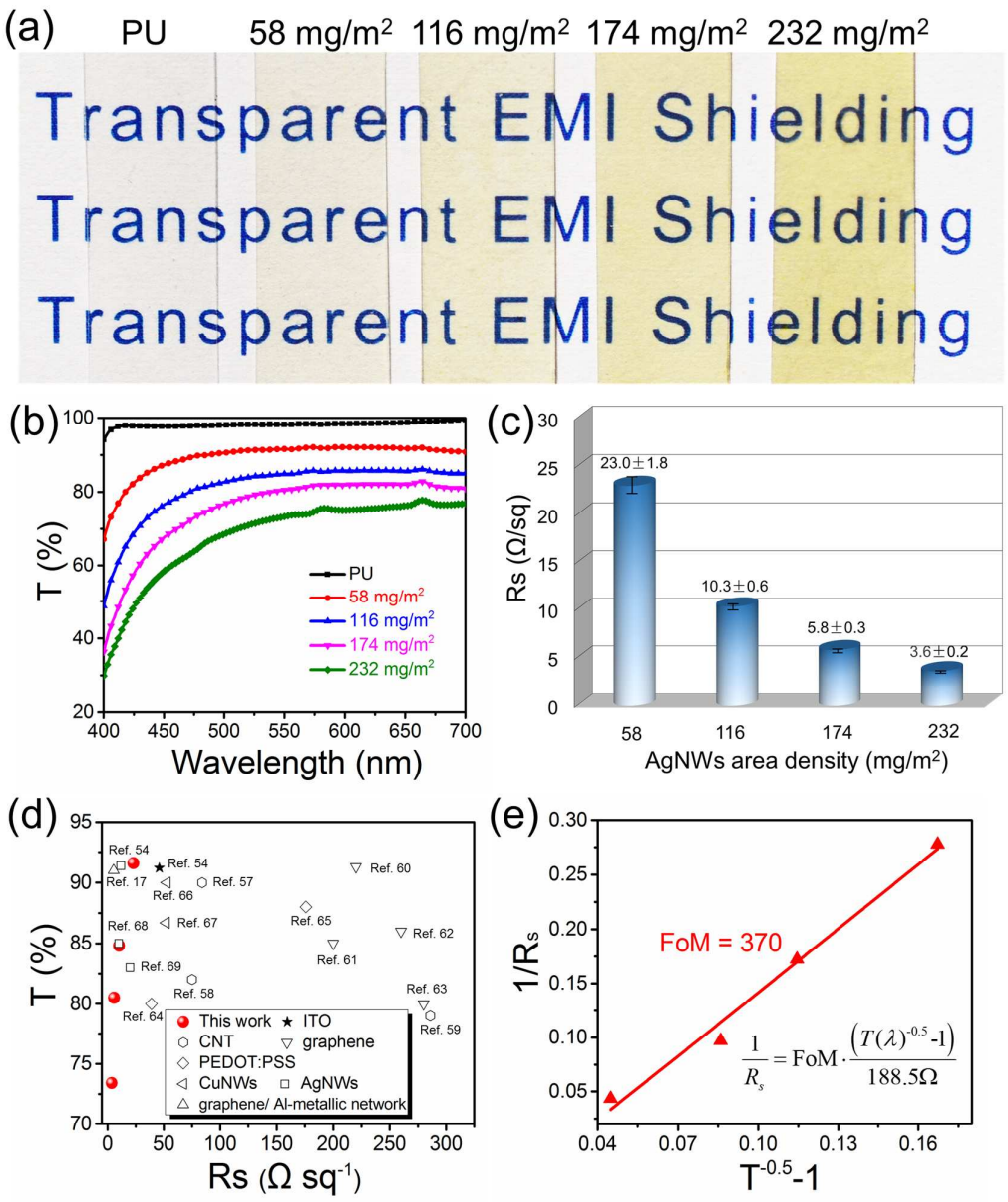

Figure 3 (a) Digital photographs of pure PU film and CA/AgNWs/PU films with different AgNW area densities. (b) Sheet resistance (Rs) of CA/AgNWs/PU films with different AgNW area densities. (c) Optical transmittance (T) of CA/AgNWs/PU films with different AgNW area densities. (d) Optical transmittance versus Rs at 550 nm for CA/AgNWs/PU films and previously reported transparent conductive films (TCFs). (e) $1/R$s plotted as a function of ($T^{-0.5}-1$) for the CA/AgNWs/PU films.

The transparent and electrical performance are critical parameters to assess the quality and practical applications for transparent EMI shielding films. Figure 3a shows digital photographs of the pure PU and CA/AgNWs/PU films with different AgNW area densities. Letters underneath all films are visible, regardless of the AgNW area density. Figure 3b presents the corresponding optical transmittance (T) of these films. The CA/AgNWs/PU films maintain a high T of between 92% and 73%, although the T value decreases with an increase in AgNW area density, due to a stronger scattering and reflection of photons. The increased AgNW area density leads to a significantly decreased R_S from 23.0 to 3.8 Ω/sq (Figure 3c), because of the closely packed AgNW networks. The T versus R_S of the CA/AgNWs/PU films is presented in Figure 3d and the corresponding value is listed in Table S1. Results for the previously reported transparent conductive films (TCFs) are presented for comparison. The integration of an R_S of 23.0 Ω/sq and a transmittance of 92% in our CA/AgNWs/PU film is superior to that for traditional ITO film (46 Ω/sq @ 91%).[54] To evaluate the opto-electrical performance of the CA/AgNWs/PU films, we calculated the figure of merit (F_OM) based on the transmittance and R_S, according to the following formula.[55,56]

$$T(\lambda) = \left(1 + \frac{Z_0}{2R_s}\frac{\sigma_{\mathrm{op}}(\lambda)}{\sigma_{\mathrm{dc}}}\right)^{-2} \qquad (1)$$

Where λ is wavelength, T is the transmittance at λ nm, Z_0 is the impedance of free space (377 Ω), $\sigma_{op}(\lambda)$ is the optical conductivity at λ nm, and σ_{dc} is the direct current conductivity. Here, FoM is taken as the ratio of the direct current conductivity to the optical conductivity, *i.e.*, $\sigma_{\mathrm{dc}}/\sigma_{\mathrm{op}}$. In general, a higher FoM results in a better

material opto-electrical performance.[37] According to formula 1, the FoM for the materials can be indicated as the following formula 2:

$$\frac{1}{R_s} = \mathrm{FoM} \cdot \frac{\left(T(\lambda)^{-0.5}\text{-}1\right)}{188.5\Omega} \qquad (2)$$

Figure 3e plotted the $1/R$s as a function of $(T^{-0.5}-1)$ for the CA/AgNWs/PU films and the FoM can be calculated from the slope of the linear fitting. Herein, the CA/AgNWs/PU films achieve a FoM of up to 370 (Figure 3e), which is comparable to or even better than that for the reported carbon nanotube, graphene, poly(ethylene dioxythiophene):poly(styrenesulfonate), and copper nanowire-based TCFs (Table S1).[17,51,54,57-69] Such a high FoM is attributed to the remarkable electrical conduction of AgNWs and the pore structure in the AgNW networks. The excellent opto-electrical performance provides the CA/AgNWs/PU films with great potential as high-performance transparent EMI shielding materials.

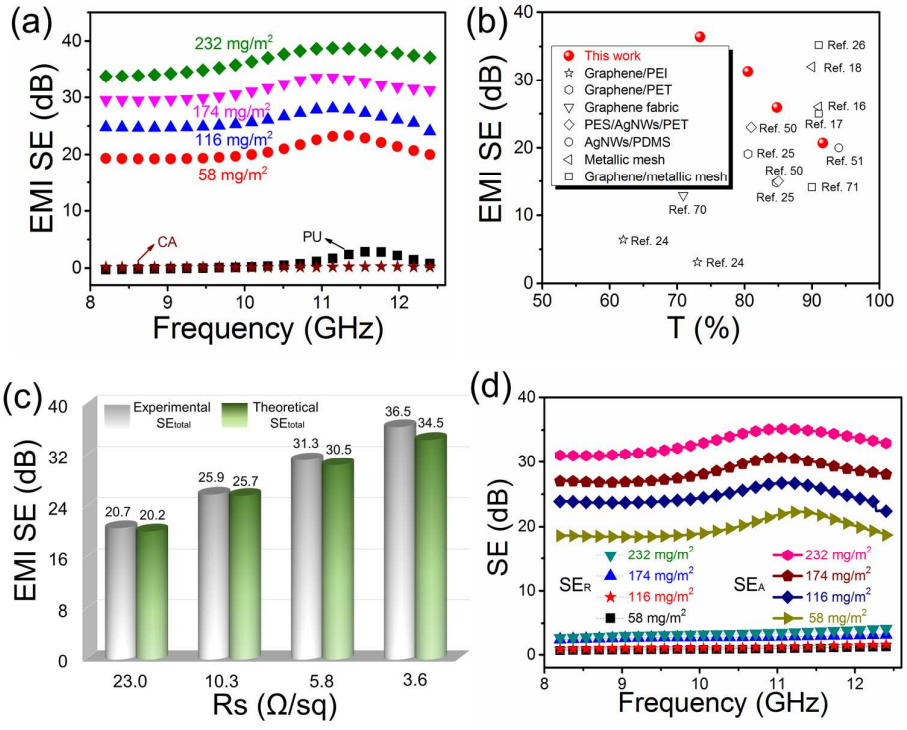

Figure 4 (a) EMI SE of the pure PU, CA and CA/AgNWs/PU films with various AgNW area densities in X-band. (b) Comparison of average EMI SE in X-band and optical transmittance (*T*) for CA/AgNWs/PU films with previously reported TCFs. (c) Experimental and theoretical EMI SE of CA/AgNWs/PU films as a function of R_S. (d) SE_R and SE_A of CA/AgNWs/PU films as a function of AgNW area density.

Figure 4a shows the EMI shielding performance of pure PU and the CA/AgNWs/PU films in X-band. Pure PU and CA are transparent to electromagnetic waves and exhibit almost no shielding ability. The CA/AgNWs/PU films show a strong EMI shielding ability, which increases with AgNW area density. This should be attribute to the reduced resistance, originating from the increased thickness of conductive AgNW layer with increasing AgNW area density. It is well established that the EMI SE of a conductive material is related to its electrical performance.[2,6] The increase in EMI SE with reduced resistance can step from the higher amount of free electrons in the CA/AgNWs/PU films that can interact with the incoming electromagnetic waves. The average EMI SE of the CA/AgNWs/PU film reaches 20.7 dB at a low AgNW area density of 58 mg/m^2. Such an EMI SE value combination with a high optical transmittance (92%) is sufficient to satisfy the requirement of a commercial transparent EMI shielding application (20 dB @ 90%).[17] As the AgNW area density increases to 116 and 174 mg/m^2, the CA/AgNWs/PU films yield an EMI SE of 25.9 and 31.3 dB, with a transmittance of 85% and 81%, respectively. As presented in Figure 4b and Table S2, our CA/AgNWs/PU films match or outperform most previously reported transparent EMI shielding materials.[16-18,24-26,50,51,70,71] Since

a broad effective bandwidth is preferable for EMI shielding applications, we also characterized the EMI SE of CA/AgNWs/PU films in C-band and Ku-band (Figure S1). It is noted that the CA/AgNWs/PU films also present excellent EMI shielding performance in the C-band and Ku-band. For example, the average EMI SE is 34.6 dB and 37.3 dB in C-band and Ku-band at an AgNW area density of 232 mg/m^2. These results indicate that more than 99.96% of the incident radiation would be eliminated within a very broad frequency range from 4 to 18 GHz.

The EMI SE exhibits a strong dependence on the electrical performance for a shielding material.[72,73] A theoretical analysis of the relationship between the EMI SE in the high frequency (higher than 30 MHz) and R_S can be carried out based on the following formulas.[19,23,74]

$$EMI\ SE = 20\log\left(1+\frac{Z_0}{2R_S}\right) \qquad (3)$$

The theoretically calculated EMI SE increases with a decreased R_S, and matches the experimental value well (Figure 4c). We established a relationship between the EMI SE and transmittance based on formulas (1) and (3), as follows:

$$EMI\ SE = 20\log\left(1+\frac{\sigma_{dc}}{\sigma_{op}(\lambda)}\left(T(\lambda)^{-0.5}-1\right)\right) \qquad (4)$$

Formula (4) can be used to optimize the tradeoff between the EMI shielding and transparent properties of the TCFs, by calculating the theoretical EMI SE of the material based on the specific transmittance for a transparent material. For example, when the AgNW area density increases to 290, 348 and 406 mg/m^2, the corresponding transmittances are 67%, 61% and 54%, respectively. Bringing the transmittances into

the formula, the corresponding theoretical EMI SEs of CA/AgNWs/PU films are 37.3, 40.0 and 42.1 dB, which are highly consist with the experimental results (Table S3). Thus, the formula (4) is of important guiding significance for the designing a technically and economically competitive transparent EMI shielding material to meet specific EMI shielding application. To ascertain the EMI shielding mechanism in the CA/AgNWs/PU films, the contribution of microwave reflection (SE_R) and microwave absorption (SE_A) to the EMI SE (SE_{total}) is shown in Figure 4d and detailed discussions are provided in Supporting Information (Figures S2 and S3). An increase in AgNW area density yields a slight increase in SE_R and a substantial increase in SE_A. The SE_A is much higher than the SE_R over the frequency range, indicating an absorption-dominant EMI shielding in the CA/AgNWs/PU films.

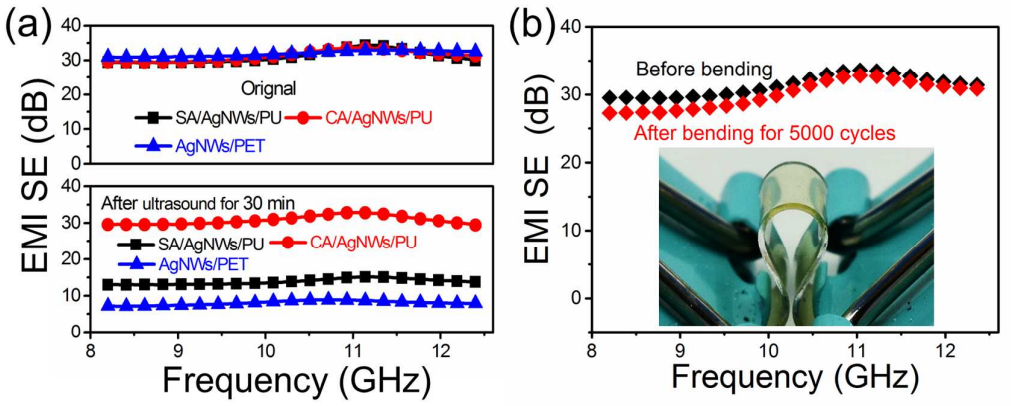

Figure 5 (a) EMI SE of CA/AgNWs/PU and SA/AgNWs/PU films before and after ultrasound treatment for 30 min. AgNWs/PET film with comparable EMI SE to CA/AgNWs/PU film was measured. (b) EMI SE variation of CA/AgNWs/PU films before and after bending to a radius of 1.5 mm for 5000 cycles. The inset shows the bending state.

Besides the high EMI SE and optical transmittance, the EMI shielding reliability to resist external forces is also a key prerequisite for a shielding material in areas of modern flexible optoelectronic systems. Thus, ultrasonic and bending tests were carried out to examine the EMI shielding robustness of the CA/AgNWs/PU film. The EMI SE of the CA/AgNWs/PU film remains essentially unchanged after ultrasound treatment for 30 min (Figure 5a). In contrast, the EMI SE of the AgNWs/PET film reveals a significant decrease from an initial value of 31.9 to 8.0 dB. The EMI SE change for the SA/AgNWs/PU film was also displayed in Figure 5a, with 17.3 dB decrease compared to the original value, indicating the destruction of the AgNW networks, which is mainly caused by the damage of water-soluble SA layer. The excellent EMI shielding robustness of the CA/AgNWs/PU film is attributed to the perfect encapsulation of AgNW networks between the water-insoluble CA and PU layers in the CA/AgNWs/PU film (Figure 2). We investigated the cyclic EMI SE durability of the CA/AgNWs/PU film before and after repeated bending (Figure 5b). The CA/AgNWs/PU film maintains a 96% EMI SE even after 5000 bending cycles, which demonstrates the excellent EMI shielding reliability. The developed CA/AgNWs/PU films exhibit a strong EMI shielding, high transmittance, and EMI shielding reliability, which provides significant potential as a high-performance transparent EMI shielding material.

4. CONCLUSION

A highly flexible and reliable transparent EMI shielding film has been demonstrated *via* a Mayer-rod coating technique. The CA/AgNWs/PU film exhibits an EMI SE of

20.7 dB and an optical transmittance of 92% at an AgNW area density of 58 mg/m^2, which is an optimal value for the shielding materials. A higher EMI SE of 31.3 dB with an optical transmittance of 81% is achieved for the composite film at a 174 mg/m^2 AgNW area density. An outstanding EMI shielding reliability with a negligible EMI SE change is observed, even after ultrasound treatment for 30 min and 5000 bending cycles. We have established a relationship between the EMI SE and optical transmittance, which is suitable for extension to a large class of transparent EMI shielding film to optimize the tradeoff between the EMI SE and the optical transmittance in specific applications. The unique attributes of our composite films demonstrate their great potential as high-performance transparent EMI shielding materials for emerging optoelectronic devices, such as flexible solar cells, displays, and touch panels.

ASSOCIATED CONTENT

Supporting Information:

The Supporting Information is available free of charge on the ACS Publications website at DOI:

The power coefficient of reflectivity (R), transmissivity (T), and absorptivity (A) as well as EMI SE (SE_{total}), microwave reflection (SE_R) and microwave absorption (SE_A) from scattering parameters; comparison of opto-electrical performance for the CA/AgNWs/PU films with other TCFs reported in the literature (Table S1); comparison of EMI SE for the CA/AgNWs/PU films with other transparent EMI shielding materials reported in the literature (Table S2); EMI shielding performance

of the CA/AgNWs/PU films in the frequency range of C-band and Ku-band; SE_{total}, SE_R and SE_A of the AgNWs/PET film; the power coefficients at the frequency of 12.4 GHz for the CA/AgNWs/PU films; experimental and theoretical EMI SE of CA/AgNWs/PU films as a function of Rs. (PDF)

AUTHOR INFORMATION

Corresponding Author

*E-mail: yandingxiang@scu.edu.cn; zmli@scu.edu.cn

Notes

The authors declare no competing financial interest.

ACKNOWLEDGEMENTS

The authors gratefully acknowledge the financial support from the National Natural Science Foundation of China (Grant No. 21704070, 51673134, 51721091), the Science and Technology Department of Sichuan Province (Grant No. 2017GZ0412), and the Fundamental Research Funds for the Central Universities (2017SCU04A03, sklpme2017306, 2012017yjsy102).

REFERENCES

(1) Thomassin, J. M.; Thomassin, J. M.; Jérôme, C.; Pardoen, T.; Bailly, C.; Huynen, I.; Detrembleur, C. Polymer/Carbon Based Composites as Electromagnetic Interference (EMI) Shielding Materials. *Mater. Sci. Eng., R,* **2013**, *74*, 211-232.

(2) Shahzad, F.; Alhabeb, M.; Hatter, C. B.; Anasori, B.; Man Hong, S.; Koo, C. M.; Gogotsi, Y. Electromagnetic Interference Shielding with 2D Transition Metal Carbides (Mxenes). *Science* **2016**, *353*, 1137-1140.

(3) Jia, L. C.; Yan, D. X.; Yang, Y.; Zhou, D.; Cui, C. H.; Bianco, E.; Lou, J.; Vajtai, R.; Li, B.; Ajayan, P. M.; Li, Z. M. High Strain Tolerant EMI Shielding Using Carbon Nanotube Network Stabilized Rubber Composite. *Adv. Mater. Technol.* **2017**, *2*, 1700078-1700083.

(4) Arjmand, M.; Chizari, K.; Krause, B.; Pötschke, P.; Sundararaj, U. Effect of Synthesis Catalyst on Structure of Nitrogen-Doped Carbon Nanotubes ond Electrical Conductivity ond Electromagnetic Interference Shielding of Their Polymeric Nanocomposites. *Carbon* **2016**, *98*, 358-372.

(5) Song, W. L.; Wang, J.; Fan, L. Z.; Li, Y.; Wang, C. Y.; Cao, M. S. Interfacial Engineering of Carbon Nanofiber–Graphene–Carbon Nanofiber Heterojunctions in Flexible Lightweight Electromagnetic Shielding Networks. *ACS Appl. Mater. Interfaces* **2014**, *6*, 10516-10523.

(6) Liu, J.; Zhang, H. B.; Sun, R.; Liu, Y.; Liu, Z.; Zhou, A.; Yu, Z. Z. Hydrophobic, Flexible, and Lightweight MXene Foams for High-Performance Electromagnetic-Interference Shielding. *Adv. Mater.* **2017**, *29*, 1702367-1702372.

(7) Song, W. L.; Cao, M. S.; Lu, M. M.; Bi, S.; Wang, C. Y.; Liu, J.; Yuan, J.; Fan, L. Z. Flexible Graphene/Polymer Composite Films in Sandwich Structures for Effective Electromagnetic Interference Shielding. *Carbon* **2014**, *66*, 67-76.

(8) Song, W. L.; Guan, X. T.; Fan, L. Z.; Cao, W. Q.; Wang, C. Y.; Zhao, Q. L.; Cao, M. S. Magnetic and Conductive Graphene Papers Toward Thin Layers of Effective Electromagnetic Shielding. *J. Mater. Chem. A* **2015**, *3*, 2097-2107.

(9) Jia, L. C.; Li, M. Z.; Yan, D. X.; Cui, C. H.; Wu, H. Y.; Li, Z. M. A Strong and Tough Polymer-Carbon Nanotube Film for Flexible and Efficient Electromagnetic Interference Shielding. *J. Mater. Chem. C* **2017**, *5*, 8944-8951.

(10) Ameli, A.; Jung, P. U.; Park, C. B. Electrical Properties and Electromagnetic Interference Shielding Effectiveness of Polypropylene/Carbon Fiber Composite Foams. *Carbon* **2013**, *60*, 379-391.

(11) Zhao, B.; Zhao, C.; Li, R.; Hamidinejad, S. M.; Park, C. B. Flexible, Ultrathin, and High-Efficiency Electromagnetic Shielding Properties of Poly (vinylidene fluoride)/Carbon Composite Films. *ACS Appl. Mater. Interfaces* **2017**, *9*, 20873–20884.

(12) Aissa, B.; Nedil, M.; Kroeger, J.; Hossain, M. I.; Mahmoud, K.; Rosei, F. Nanoelectromagnetic of the N-Doped Single Wall Carbon Nanotube in the Extremely High Frequency Band. *Nanoscale* **2017,** *9*, 14192-14200.

(13) Jia, L. C.; Li, Y. K.; Yan, D. X. Flexible and Efficient Electromagnetic Interference Shielding Materials From Ground Tire Rubber. *Carbon* **2017**, *121*, 267-273.

(14) Shen, B.; Li, Y.; Yi, D.; Zhai, W.; Wei, X.; Zheng, W. Strong Flexible Polymer/Graphene Composite Films with 3D Saw-Tooth Folding for Enhanced and Tunable Electromagnetic Shielding. *Carbon* **2017**, *113*, 55-62.

(15) Lee, S. H.; Yu, S.; Shahzad, F.; Kim, W. N.; Park, C.; Hong, S. M.; Koo, C. M. Density-Tunable Lightweight Polymer Composites with Dual-Functional Ability of Efficient EMI Shielding and Heat Dissipation. *Nanoscale* **2017**, *9*,

13432-13440.

(16) Han, Y.; Lin, J.; Liu, Y.; Fu, H.; Ma, Y.; Jin, P.; Tan, J. Crackle Template Based Metallic Mesh with Highly Homogeneous Light Transmission for High-Performance Transparent EMI Shielding. *Sci*. *Rep*. **2016**, *6*, 25601-25611.

(17) Ma, L.; Lu, Z.; Tan, J.; Liu, J.; Ding, X.; Black, N.; Li, T.; Gallop, J.; Hao, L. Transparent Conducting Graphene Hybrid Films To Improve Electromagnetic Interference (EMI) Shielding Performance of Graphene. *ACS Appl*. *Mater*. *Interfaces* **2017**, *9*, 34221-34229.

(18) Wang, H.; Lu, Z.; Liu, Y.; Tan, J.; Ma, L.; Lin, S. Double-Layer Interlaced Nested Multi-Ring Array Metallic Mesh for High-Performance Transparent Electromagnetic Interference Shielding. *Opt. Lett.* **2017,** *42*, 1620-1623.

(19) Maniyara, R. A.; Mkhitaryan, V. K.; Chen, T. L.; Ghosh, D. S.; Pruneri, V. An Antireflection Transparent Conductor with Ultralow Optical Loss (< 2%) and Electrical Resistance (< 6 Ω Sq^{-1}). *Nature Commun.* **2016,** *7*, 13771.

(20) Xu, H.; Anlage, S. M.; Hu, L.; Gruner, G. Microwave Shielding of Transparent and Conducting Single-Walled Carbon Nanotube Films. *Appl*. *Phys*. *Lett*. **2007**, *90*, 183119-183121.

(21) Hong, S. K.; Kim, K. Y.; Kim, T. Y.; Kim, J. H.; Park, S. W.; Cho, B. J. Electromagnetic Interference Shielding Effectiveness 0f Monolayer Graphene. *Nanotechnology* **2012**, *23*, 455704-455708.

(22) Choi, Y. J.; Gong, S. C.; Johnson, D. C.; Golledge, S.; Yeom, G. Y.; Park, H. H. Characteristics of the Electromagnetic Interference Shielding Effectiveness of

Al-Doped Zno Thin Films Deposited by Atomic Layer Deposition. *Appl. Surf. Sci.* **2013**, *269*, 92-97.

(23) Kim, B.; Lee, H.; Kim, E.; Lee, S. H. Intrinsic Electromagnetic Radiation Shielding/Absorbing Characteristics of Polyaniline-Coated Transparent Thin Films. *Synthetic Met.* **2010**, *160*, 1838-1842.

(24) Kim, S.; Oh, J. S.; Kim, M. G.; Jang, W.; Wang, M.; Kim, Y.; Seo, H. W.; Kim, Y. C.; Lee, J. H.; Lee, Y. Electromagnetic Interference (EMI) Transparent Shielding of Reduced Graphene Oxide (RGO) Interleaved Structure Fabricated by Electrophoretic Deposition. *ACS Appl. Mater. Interfaces* **2014**, *6*, 17647-17653.

(25) Lu, Z.; Ma, L.; Tan, J.; Wang, H.; Ding, X. Transparent Multi-Layer Graphene/Polyethylene Terephthalate Structures with Excellent Microwave Absorption and Electromagnetic Interference Shielding Performance. *Nanoscale* **2016**, *8*, 16684-16693.

(26) Lu, Z.; Ma, L.; Tan, J.; Wang, H.; Ding, X. Graphene, Microscale Metallic Mesh, and Transparent Dielectric Hybrid Structure for Excellent Transparent Electromagnetic Interference Shielding and Absorbing. *2D Mater.* **2017**, *4*, 025021-025028.

(27) Kim, D. H.; Yu, K. C.; Kim, Y.; Kim, J. W. Highly Stretchable and Mechanically Stable Transparent Electrode Based on Composite of Silver Nanowires and Polyurethane–Urea. *ACS Appl. Mater. Interfaces* **2015**, *7*, 15214-15222.

(28) Liang, J.; Li, L.; Tong, K.; Ren, Z.; Hu, W.; Niu, X.; Chen, Y.; Pei, Q. Silver Nanowire Percolation Network Soldered with Graphene Oxide at Room

Temperature and Its Application for Fully Stretchable Polymer Light-Emitting Diodes. *ACS Nano* **2014**, *8*, 1590-1600.

(29) Lee, J. G.; Kim, D. Y.; Lee, J. H.; Sinha-Ray, S.; Yarin, A. L.; Swihart, M. T.; Kim, D.; Yoon, S. S. Production of Flexible Transparent Conducting Films of Self-Fused Nanowires via One-Step Supersonic Spraying. *Adv. Funct. Mater.* **2017**, *27*, 1602548-1602554.

(30) Kim, D. H.; Kim, Y.; Kim, J. W. Transparent and Flexible Film for Shielding Electromagnetic Interference. *Mater. Des.* **2016,** *89*, 703-707.

(31) Jin, Y.; Wang, K.; Cheng, Y.; Pei, Q.; Xu, Y.; Xiao, F. Removable Large-Area Ultrasmooth Silver Nanowire Transparent Composite Electrode. *ACS Appl. Mater. Interfaces* **2017**, *9*, 4733-4741.

(32) Lee, J.; Lee, P.; Lee, H.; Lee, D.; Lee, S. S.; Ko, S. H. Very Long Ag Nanowire Synthesis and Its Application In a Highly Transparent, Conductive and Flexible Metal Electrode Touch Panel. *Nanoscale* **2012**, *4*, 6408-6414.

(33) Liang, J.; Li, L.; Niu, X.; Yu, Z.; Pei, Q. Elastomeric Polymer Light-Emitting Devices and Displays. *Nature Photon*. **2013**, *7*, 817-824.

(34) Hong, S.; Lee, H.; Lee, J.; Kwon, J.; Han, S.; Suh, Y. D.; Cho, H.; Shin, J.; Yeo, J.; Ko, S. H. Highly Stretchable and Transparent Metal Nanowire Heater for Wearable Electronics Applications. *Adv. Mater.* **2015**, *27*, 4744-4751.

(35) Jeong, C. K.; Lee, J.; Han, S.; Ryu, J.; Hwang, G. T.; Park, D. Y.; Park, J. H.; Lee, S. S.; Byun, M.; Ko, S. H. A Hyper-Stretchable Elastic-Composite Energy Harvester. *Adv. Mater.* **2015,** *27*, 2866-2875.

(36) Moon, H.; Lee, H.; Kwon, J.; Suh, Y. D.; Kim, D. K.; Ha, I.; Yeo, J.; Hong, S.; Ko, S. H. Ag/Au/Polypyrrole Core-Shell Nanowire Network for Transparent, Stretchable and Flexible Supercapacitor in Wearable Energy Devices. *Sci. Rep.* **2017,** *7*, 41981.

(37) Lee, H.; Hong, S.; Lee, J.; Suh, Y. D.; Kwon, J.; Moon, H.; Kim, H.; Yeo, J.; Ko, S. H. Highly Stretchable and Transparent Supercapacitor by Ag–Au Core–Shell Nanowire Network with High Electrochemical Stability. *ACS Appl. Mater. Interfaces* **2016,** *8*, 15449-15458.

(38) Chang, I.; Park, T.; Lee, J.; Lee, M. H.; Ko, S. H.; Cha, S. W. Bendable Polymer Electrolyte Fuel Cell Using Highly Flexible Ag Nanowire Percolation Network Current Collectors. *J. Mater. Chem. A* **2013,** *1*, 8541-8546.

(39) Chang, I.; Park, T.; Lee, J.; Lee, H. B.; Ji, S.; Lee, M. H.; Ko, S. H.; Cha, S. W. Performance Enhancement in Bendable Fuel Cell Using Highly Conductive Ag Nanowires. *Int. J Hydrogen Energ.* **2014,** *39*, 7422-7427.

(40) Chang, I.; Park, T.; Lee, J.; Lee, H. B.; Ko, S. H.; Cha, S. W. Flexible Fuel Cell Using Stiffness-Controlled Endplate. *Int. J Hydrogen Energ.* **2016,** *41*, 6013-6019.

(41) Kim, K. K.; Hong, S.; Cho, H. M.; Lee, J.; Suh, Y. D.; Ham, J.; Ko, S. H. Highly Sensitive and Stretchable Multidimensional Strain Sensor with Prestrained Anisotropic Metal Nanowire Percolation Networks. *Nano Lett.* **2015,** *15*, 5240-5247.

(42) Lee, P.; Lee, J.; Lee, H.; Yeo, J.; Hong, S.; Nam, K. H.; Lee, D.; Lee, S. S.; Ko, S.

H. Highly Stretchable and Highly Conductive Metal Electrode by Very Long Metal Nanowire Percolation Network. *Adv. Mater.* **2012,** *24*, 3326-3332.

(43) Jeong, S.; Cho, H.; Han, S.; Won, P.; Lee, H.; Hong, S.; Yeo, J.; Kwon, J.; Ko, S. H. High Efficiency, Transparent, Reusable, and Active PM2. 5 Filters by Hierarchical Ag Nanowire Percolation Network. *Nano Lett.* **2017,** *17*, 4339-4346.

(44) HwanáKo, S. A Dual-Scale Metal Nanowire Network Transparent Conductor for Highly Efficient and Flexible Organic Light Emitting Diodes. *Nanoscale* **2017,** *9*, 1978-1985.

(45) Moon, H.; Won, P.; Lee, J.; Ko, S. H. Low-Haze, Annealing-Free, Very Long Ag Nanowire Synthesis and Its Application in a Flexible Transparent Touch Panel. *Nanotechnology* **2016,** *27*, 295201.

(46) Hong, S.; Yeo, J.; Lee, J.; Lee, H.; Lee, P.; Lee, S. S.; Ko, S. H. Selective Laser Direct Patterning of Silver Nanowire Percolation Network Transparent Conductor for Capacitive Touch Panel. *J. Nanosci. Nanotechno.* **2015,** *15*, 2317-2323.

(47) Lee, P.; Ham, J.; Lee, J.; Hong, S.; Han, S.; Suh, Y. D.; Lee, S. E.; Yeo, J.; Lee, S. S.; Lee, D. Highly Stretchable or Transparent Conductor Fabrication by a Hierarchical Multiscale Hybrid Nanocomposite. *Adv. Funct. Mater.* **2014,** *24*, 5671-5678.

(48) Lee, J.; Lee, P.; Lee, H. B.; Hong, S.; Lee, I.; Yeo, J.; Lee, S. S.; Kim, T. S.; Lee, D.; Ko, S. H. Room-Temperature Nanosoldering of a Very Long Metal Nanowire Network by Conducting-Polymer-Assisted Joining for a Flexible Touch-Panel Application. *Adv. Funct. Mater.* **2013,** *23*, 4171-4176.

(49) Lee, J. H.; Lee, P.; Lee, D.; Lee, S. S.; Ko, S. H. Large-Scale Synthesis and Characterization of Very Long Silver Nanowires via Successive Multistep Growth. *Cryst. Growth Des.* **2012,** *12*, 5598-5605.

(50) Hu, M.; Gao, J.; Dong, Y.; Li, K.; Shan, G.; Yang, S.; Li, R. K. Y. Flexible Transparent PES/Silver Nanowires/PET Sandwich-Structured Film for High-Efficiency Electromagnetic Interference Shielding. *Langmuir* **2012**, *28*, 7101-7106.

(51) Jung, J.; Lee, H.; Ha, I.; Cho, H.; Kim, K. K.; Kwon, J.; Won, P.; Hong, S.; Ko, S. H. Highly Stretchable and Transparent Electromagnetic Interference Shielding Film Based on Silver Nanowire Percolation Network for Wearable Electronics Applications. *ACS Appl. Mater. Interfaces* **2017,** *9*, 44609-44616.

(52) Yan, D. X.; Pang, H.; Li, B.; Vajtai, R.; Xu, L.; Ren, P. G.; Wang, J. H.; Li, Z. M., Structured Reduced Graphene Oxide/Polymer Composites for Ultra-Efficient Electromagnetic Interference Shielding. *Adv. Funct. Mater.* **2015**, *25*, 559-566.

(53) Lee, J.; Lim, M.; Yoon, J.; Kim, M. S.; Choi, B.; Kim, D. M.; Kim, D. H.; Park, I.; Choi, S. J. Transparent, Flexible Strain Sensor Based on a Solution-Processed Carbon Nanotube Network. *ACS Appl. Mater. Interfaces* **2017**, *9*, 26279-26285.

(54) Song, M.; You, D. S.; Lim, K.; Park, S.; Jung, S.; Kim, C. S.; Kim, D. H.; Kim, D. G.; Kim, J. K.; Park, J. Highly Efficient and Bendable Organic Solar Cells with Solution-Processed Silver Nanowire Electrodes. *Adv. Funct. Mater.* **2013**, *23*, 4177-4184.

(55) He, L.; Tjong, S. C. Nanostructured Transparent Conductive Films: Fabrication,

Characterization and Applications. *Mater. Sci. Eng., R,* **2016**, *109*, 1-101.

(56) McCoul, D.; Hu, W.; Gao, M.; Mehta, V.; Pei, Q. Recent Advances in Stretchable and Transparent Electronic Materials. *Adv*. *Electro*. *Mater*. **2016**, *2*, 1500407-1500457.

(57) Geng, H. Z.; Lee, D. S.; Kim, K. K.; Han, G. H.; Park, H. K.; Lee, Y. H. Absorption Spectroscopy of Surfactant-Dispersed Carbon Nanotube Film: Modulation of Electronic Structures. *Chem*. *Phys*. *Lett*. **2008**, *455*, 275-278.

(58) Li, X.; Gittleson, F.; Carmo, M.; Sekol, R. C.; Taylor, A. D. Scalable Fabrication of Multifunctional Freestanding Carbon Nanotube/Polymer Composite Thin Films for Energy Conversion. *ACS Nano* **2012**, *6*, 1347-1356.

(59) Cho, D. Y.; Eun, K.; Choa, S. H.; Kim, H. K. Highly Flexible and Stretchable Carbon Nanotube Network Electrodes Prepared by Simple Brush Painting for Cost-Effective Flexible Organic Solar Cells. *Carbon* **2014**, *66*, 530-538.

(60) Ryu, J.; Kim, Y.; Won, D.; Kim, N.; Park, J. S.; Lee, E. K.; Cho, D.; Cho, S. P.; Kim, S. J.; Ryu, G. H.; Shin, H. A. S.; Lee, Z.; Hong, B. H.; Cho, S. Fast Synthesis of High-Performance Graphene Films by Hydrogen-Free Rapid Thermal Chemical Vapor Deposition. *ACS Nano* **2014**, *8*, 950-956.

(61) Cai, W.; Zhu, Y.; Li, X.; Piner, R. D.; Ruoff, R. S. Large Area Few-Layer Graphene/Graphite Films as Transparent Thin Conducting Electrodes. *Appl*. *Phys*. *Lett*. **2009**, *95*, 123115-123117.

(62) Majee, S.; Song, M.; Zhang, S. L.; Zhang, Z. B. Scalable Inkjet Printing Of Shear-Exfoliated Graphene Transparent Conductive Films. *Carbon* **2016**, *102*,

51-57.

(63) Kim, K. S.; Zhao, Y.; Jang, H.; Lee, S. Y.; Kim, J. M.; Kim, K. S.; Ahn, J. H.; Kim, P.; Choi, J. Y.; Hong, B. H. Large-Scale Pattern Growth Of Graphene Films For Stretchable Transparent Electrodes. *Nature* **2009**, *457*, 706-710.

(64) Xia, Y.; Sun, K.; Ouyang, J. Solution-Processed Metallic Conducting Polymer Films as Transparent Electrode of Optoelectronic Devices. *Adv. Mater.* **2012**, *24*, 2436-2440.

(65) Kim, Y. H.; Sachse, C.; Machala, M. L.; May, C.; Müller-Meskamp, L.; Leo, K. Highly Conductive PEDOT:PSS Electrode with Optimized Solvent and Thermal Post-Treatment for ITO-Free Organic Solar Cells. *Adv. Funct. Mater.* **2011**, *21*, 1076-1081.

(66) Chu, H. C.; Chang, Y. C.; Lin, Y.; Chang, S. H.; Chang, W. C.; Li, G. A.; Tuan, H. Y. Spray-Deposited Large-Area Copper Nanowire Transparent Conductive Electrodes and Their Uses for Touch Screen Applications. *ACS Appl. Mater. Interfaces* **2016**, *8*, 13009-13017.

(67) Hu, W.; Wang, R.; Lu, Y.; Pei, Q. An Elastomeric Transparent Composite Electrode Based on Copper Nanowires and Polyurethane. *J. Mater. Chem. C* **2014**, *2*, 1298-1305.

(68) Madaria, A. R.; Kumar, A.; Ishikawa, F. N.; Zhou, C. Uniform, Highly Conductive, and Patterned Transparent Films of A Percolating Silver Nanowire Network on Rigid and Flexible Substrates Using a Dry Transfer Technique. *Nano Res.* **2010**, *3*, 564-573.

(69) Liu, H. S.; Pan, B. C.; Liou, G. S. Highly Transparent Agnw/PDMS Stretchable Electrodes for Elastomeric Electrochromic Devices. *Nanoscale* **2017**, *9*, 2633-2639.

(70) Han, J.; Wang, X.; Qiu, Y.; Zhu, J.; Hu, P. Infrared-Transparent Films Based on Conductive Graphene Network Fabrics for Electromagnetic Shielding. *Carbon* **2015**, *87*, 206-214.

(71) Han, Y.; Liu, Y.; Han, L.; Lin, J.; Jin, P. High-Performance Hierarchical Graphene/Metal-Mesh Film for Optically Transparent Electromagnetic Interference Shielding. *Carbon* **2017**, *115*, 34-42.

(72) Chen, Y.; Zhang, H. B.; Yang, Y.; Wang, M.; Cao, A.; Yu, Z. Z. High-Performance Epoxy Nanocomposites Reinforced with Three-Dimensional Carbon Nanotube Sponge for Electromagnetic Interference Shielding. *Adv. Funct. Mater.* **2016**, *26*, 447-455.

(73) Jia, L. C.; Yan, D. X.; Cui, C. H.; Jiang, X.; Ji, X.; Li, Z. M. Electrically Conductive and Electromagnetic Interference Shielding of Polyethylene Composites with Devisable Carbon Nanotube Networks. *J. Mater. Chem. C* **2015**, *3*, 9369-9378.

(74) Colaneri, N. F.; Schacklette, L. EMI Shielding Measurements of Conductive Polymer Blends. *IEEE T. Instrum. Meas.* **1992**, *41*, 291-297.

Table of Contents